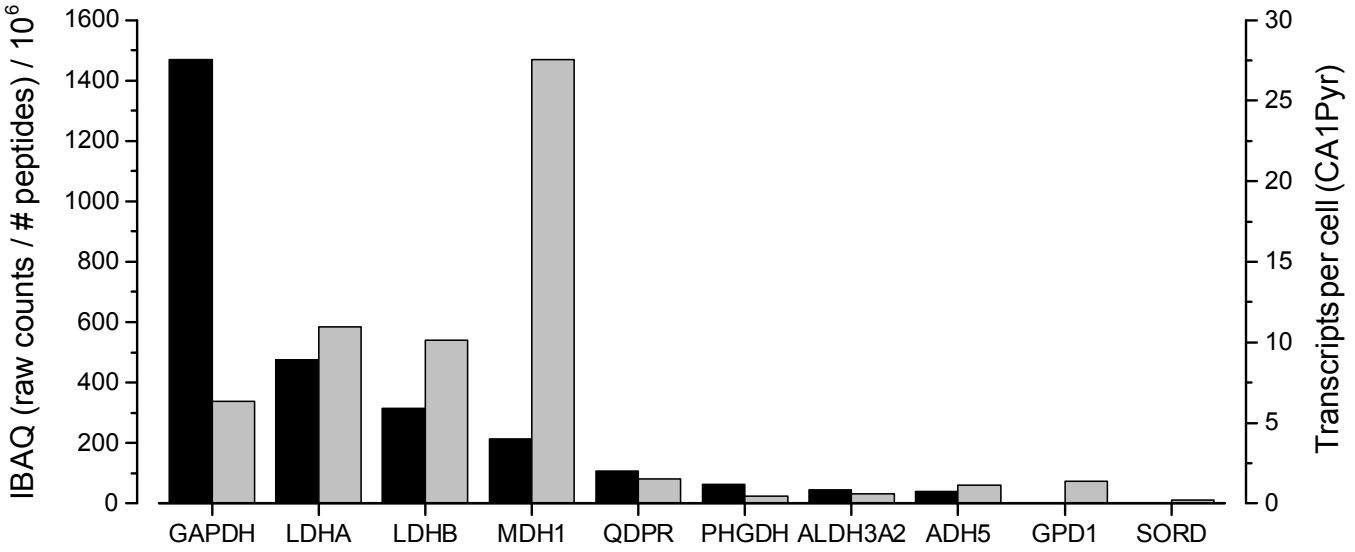

Figure S1. Relative abundance of cytosolic NADH-specific dehydrogenases in neurons. Related to Figure 1.

The graph shows the most highly abundant cytosolic NADH-specific dehydrogenases in mouse neurons, from unbiased proteomic analysis of cultured neurons (black bars, left axis; Sharma et al. 2015) and from unbiased transcriptomic analysis (single-cell RNA-seq) on CA1 pyramidal neurons (grey bars, right axis; Zeisel et al. 2015). The x-axis shows the gene names.

By far the four dominant dehydrogenases are GAPDH, LDHA/LDHB, and MDH1, corresponding to the three main $NADH_{CYT}$-controlling processes in Figure 1E. The second mitochondrial NADH shuttle, the glycerol phosphate shuttle, uses the GPD1 dehydrogenase, expressed a much lower levels than MDH1.

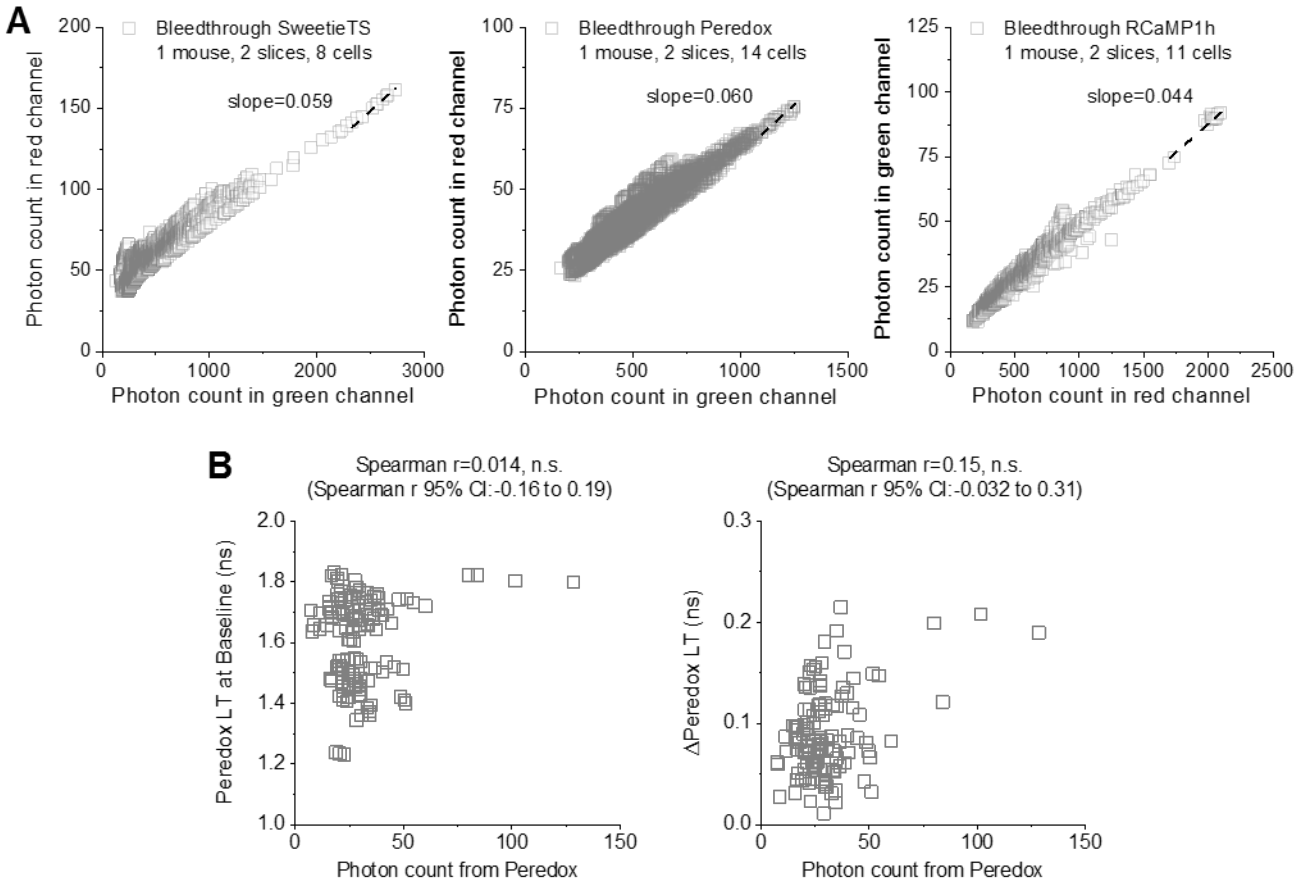

Figure S2. Bleedthrough correction and buffering effects of sensor expression. Related to Figure 1.

(**A**) Bleedthrough correction was performed in DGNs exclusively expressing one sensor. The spectral contamination of photons emitted by the green-fluorescent proteins SweetieTS and Peredox into the red channel was calculated as the slope from the linear fit of the relationship between the photon count in the red channel (left Y-axis) *versus* the photon count in the green channel (X-axis). For the fitting, at least ten points within the 80^{th}-100^{th} percentiles of photon count in the green channel were used because of a better signal to noise ratio in this range. Bleedthrough from RCaMP fluorescence to the green channel was analyzed in a similar way, although it must be taken into account that it does not reflect the spectral contamination of photons emitted by the red proteins, but the emission of immature RCaMP proteins that emit in the green spectrum. The values of bleedthrough correction for each sensor (slope) appear embedded in the graphs.

(**B**) Peredox expression does not buffer NADH or NAD^+ concentrations. No correlation was observed between the photon count of Peredox fluorescence (used as a proxy for Peredox expression in DGNs) and the Peredox lifetimes at baseline. Likewise, the magnitude of the change in Peredox lifetime in response to antidromic stimulation was not correlated with Peredox expression in DGNs (events=132, neurons=49, slices=9, mice=6).

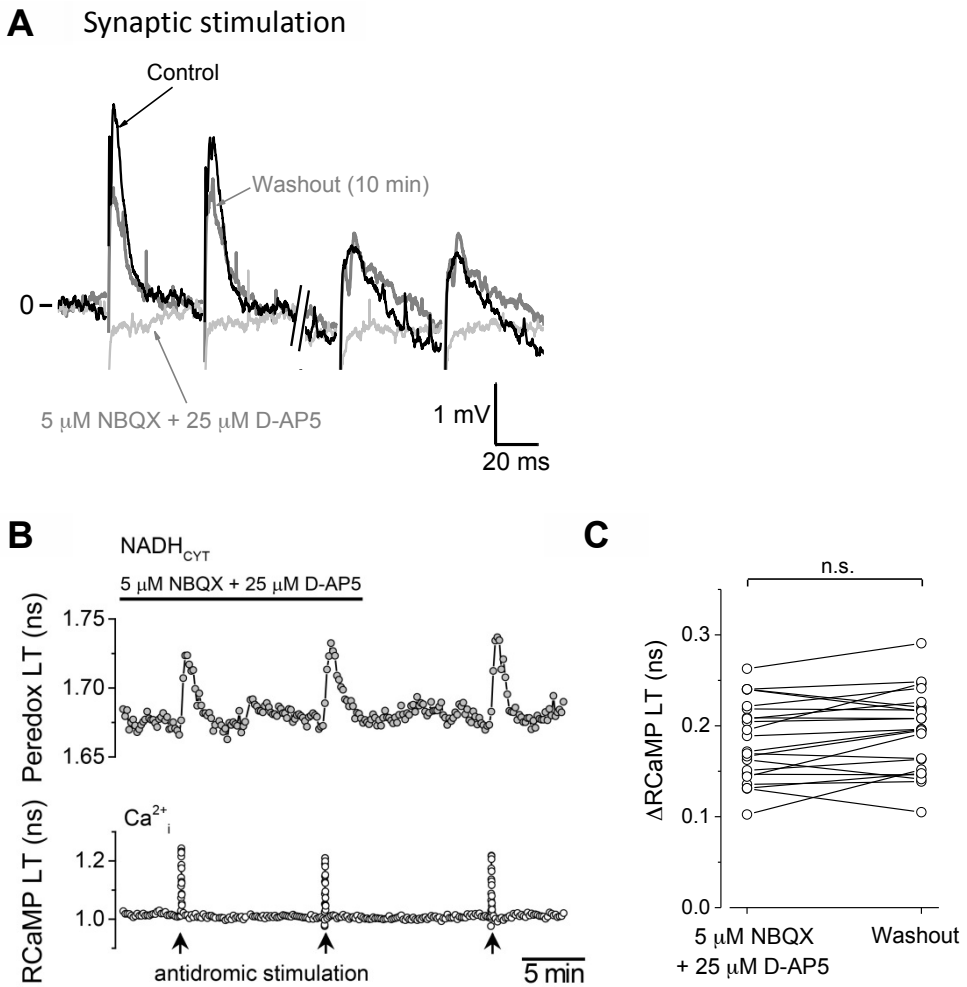

Figure S3. Effects of ionotropic glutamate receptor blockers on synaptically and antidromically stimulated DGNs. Related to Figure 2.

(**A**) Representative traces of excitatory local field potentials (LFP) recorded in dentate granule neurons after synaptic stimulation. LFPs recorded in regular ACSF (Control) were abolished by the application of ionotropic glutamate receptor blockers (5 μM NBQX + 25 μM D-AP5). LFPs were recovered after the washout of synaptic blockers from the ACSF. The trace shows a couple of LFPs at the beginning and the end in a typical stimulation train. The stimulation artifacts are blanked for better visualization of the signals.

(**B**) Representative trace of $NADH_{CYT}$ and Ca^{2+} transients elicited by antidromic stimulation, before and after washout (10 min) of synaptic blockers in the ACSF.

(**C**) As expected, the removal of synaptic blockers from the ACSF does not affect the changes in RCaMP LT induced by antidromic stimulation. Data were compared by a paired Student's t-test (neurons=22, slices=4, mice=2) and differences between both conditions were not significant (n.s.).

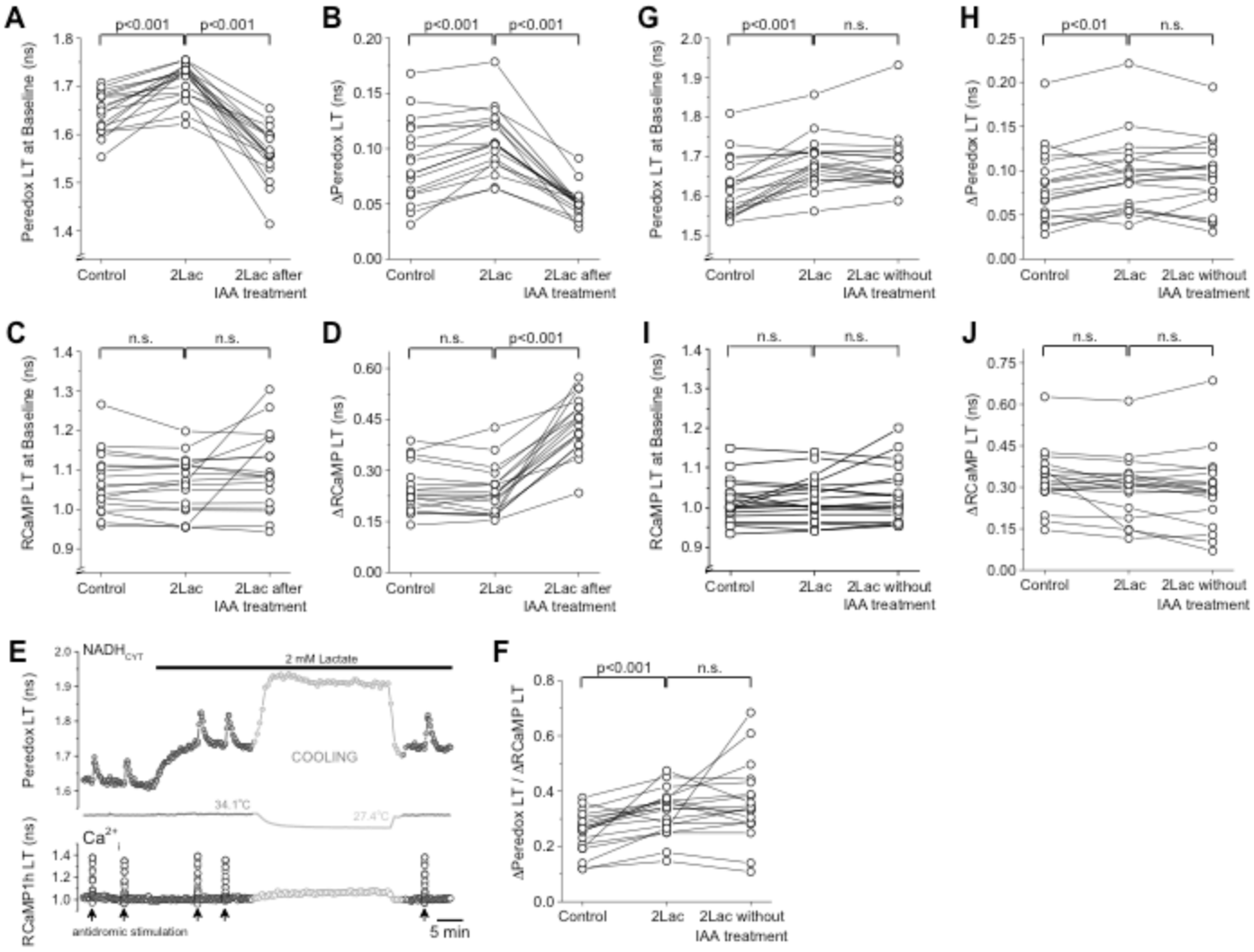

Figure S4. Further analysis of IAA and temperature shifts. Related to Figure 4.

(**A**) Peredox lifetime at baseline increases with the addition of 2 mM lactate (2Lac), as expected from the conversion of lactate to pyruvate mediated by the enzyme LDH. IAA treatment reduces the Peredox LT at levels even lower than the initial values without lactate supplementation, indicating the occurrence of neuronal glycolysis at baseline. Data were compared by a paired Student's t-test (neurons=18, slices=5, mice=5).

(**B**) Absolute Peredox lifetime changes (ΔPeredox LT) upon stimulation are slightly but significantly enhanced by lactate supplementation in the ACSF, but IAA treatment drastically reduces the metabolic $NADH_{CYT}$ responses, indicating that glycolysis is a major contributor for these transients.

(**C**) The intracellular Ca^{2+} concentration at rest is not affected by our protocol for IAA treatment. This means that the slice health was not compromised at baseline.

(**D**) Ca^{2+} transients are enhanced after IAA treatment, suggesting that the cells are more excitable or less effective in extruding (or buffering) this ion upon stimulation.

(**E**) Representative trace of $NADH_{CYT}$ transients obtained under the same conditions as in Fig 4, but without IAA treatment. The bar indicates the time of application of lactate (2 mM) and the temperature was lowered (shaded zone) to mimic the protocol for IAA application. (Temperature affects sensor lifetime directly, which is why there are large changes in the sensors' response during the temperature changes.) After returning to near-physiologic temperature, Ca^{2+} spikes and $NADH_{CYT}$ transients remained unaltered, indicating that the reduction in $NADH_{CYT}$

transients observed after IAA treatment is attributable to GAPDH inhibition and not because of a collateral effect of manipulating the temperature of the slices.

(**F**) Addition of 2 mM lactate slightly increases the magnitude of neuronal $NADH_{CYT}$ transients with respect to the extent of neuronal excitation, measured as the change in RCaMP LT. Moreover, the proportional $NADH_{CYT}$ response to Ca^{2+} transients (ΔPeredox LT / ΔRCaMP LT) remained unchanged after transiently cooling the slices. Data were compared by a paired Student's t-test (neurons=19, slices=4, mice=4).

(**G**) Peredox lifetime at baseline is not affected by changes in temperature during the protocol used in Fig 4.

(**H**) Absolute Peredox lifetime changes (ΔPeredox LT) remain the same throughout the experiments.

(**I**) The intracellular Ca^{2+} concentration at rest is not affected by the experimental paradigm. This means that the slice health was not compromised at baseline because of temperature changes.

(**J**) Ca^{2+} responses to stimulation also remained unaltered, indicating no changes in neuronal excitability or Ca^{2+} handling after the transient change in temperature.

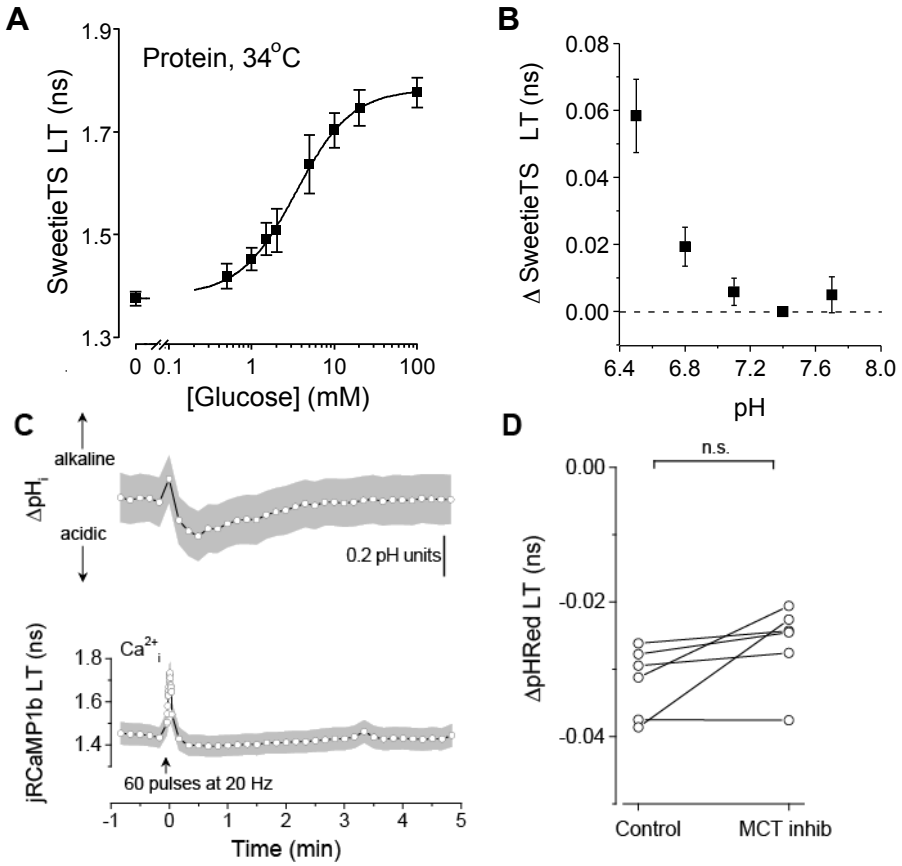

E

MRGSHHHHHH GMASMTGGQQ MGRDLYDDDD KDRWGSKLEI FSWWAGDEGP ALEALIRLYK
QKYPGVEVIN ATVTGGAGVN ARAVLKTRML GGDPPDTFQV AAGMELIGTW VVANRMEDLS
ALFRQEGWLQ AFPKGLIDLI SYKGGIWSVP VNIHRSNVMW YLPAKLKEWG VNPPRTWDEF
LATCQTLKQK GLEAPLALGE NWTQQHLWES VALAVLGPDD WNNLWNGKLK FTDPKAVRAW
EVFGRVLDCA NKDAAGLSWQ QAVDRVVQGK AAFNVMGDWA AGYMTTTLKL KPGTDFAWAP
SPGTQGVFMM LSDSFGLPKG AKNRQNAINW LRLVGSKEGQ DTFNPLKGSI AARLDSDPSK
YPDSFTAHNV YIMADKQKNG IKANFKIRHN IEDGGVQLAD HYQQNTPIGD GPVLLPDNHY
LSIQSKLSKD PNEKRDHMVL LEFVTAAGIT HGMDELYKGG TGGSMVSKGE ELFTGVVPIL
VELDGDVNGH KFSVSGEGEG DATYGKLTLK FICTTGKLPV PWPTLVTTFS YGVMVFARYP
DHMKQHDFFK SAMPEGYVQE RTIFFKDDGN YKTRAEVKFE GDTLVNRIEL KGIDFKEDGN
ILGHKLEYNE PNAYGQSAMR DWRSNRIVGS LVAGAVAPES FMSQFGTVME IFLQTRNPQA
AANAAQAIAD QVGLGRLGQ

Figure S5. Properties of the SweetieTS glucose sensor, and direction of pH responses with stimulation. Related to Figure 5.

(**A**) Calibration of the purified glucose sensor SweetieTS at near-physiologic temperature (34°C). Data represent the average of three independent experiments. The curve resulted from averaging individual fittings of each experimental dataset to a Hill equation, yielding a Km= 3.4 ± 0.7 mM for glucose and a Hill coefficient of n=1.28 ± 0.03 (mean ± SD).

(**B**) pH dependence of SweetieTS. pH dose response curves were constructed at three different glucose concentrations (0.5mM, 1mM, 3mM) for two independent purified protein samples at 34°C. For the 3 glucose concentrations tested, the lifetime of SweetieTS increased with acidification – neuronal stimulation produces a small

acidification (see C below), and any acidification-induced change in SweetieTS lifetime is in the opposite direction from the observed dips in sensor lifetime (interpreted as dips in [glucose]). Measurements were normalized to SweetieTS lifetime at pH7.4 for each glucose concentration. Data are mean ± SEM.

(**C**) DGNs show a small acidification with stimulation. The pH sensor pHRed (Tantama et al., 2011) was expressed in DGNs under the universal promoter CAG using an AAV2/8 vector. Neuronal activity was detected using the Ca^{2+} sensor jRCaMP1b (Dana et al., 2016), which was co-expressed by infecting DGNs with AAV2/9 viruses using the neuron-specific promoter synapsin. As both sensors emit in the red spectrum, cross-contamination between their signals was minimized by targeting pHRed and jRCaMP1b to the nucleus and cytoplasm respectively. Signals from both sensors can be also distinguished by their baseline lifetime values, which in our experimental conditions were pHRed LT= 2.14 ± 0.10 ns and jRCaMP1b= 1.45 ± 0.25 ns (mean ± SD from events=23, neurons=10, slices=5, mice=3). The average pH response (mean ± SEM) to synaptic stimulation (60 pulses, 100 μs of duration and 400-500 μA of intensity, delivered at 20Hz) shows a small transient intracellular acidification, as calculated using the calibration curve previously reported for pHRed lifetimes (Tantama et al., 2011). Sensors were imaged using a 2p excitation wavelength of 850 nm.

(**D**) Monocarboxylate inhibition (MCT inhib) by 2 μM AR-C155858 does not affect the magnitude of the synaptically-stimulated acidification in the intracellular pH of DGNs. Data for the effect of MCT inhibition were compared by a paired Student's t-test (neurons=6, slices=4, mice=3).

(**E**) Amino acid sequence of the SweetieTS sensor. The sequence of the circularly-permuted variant of TSapphire is highlighted.

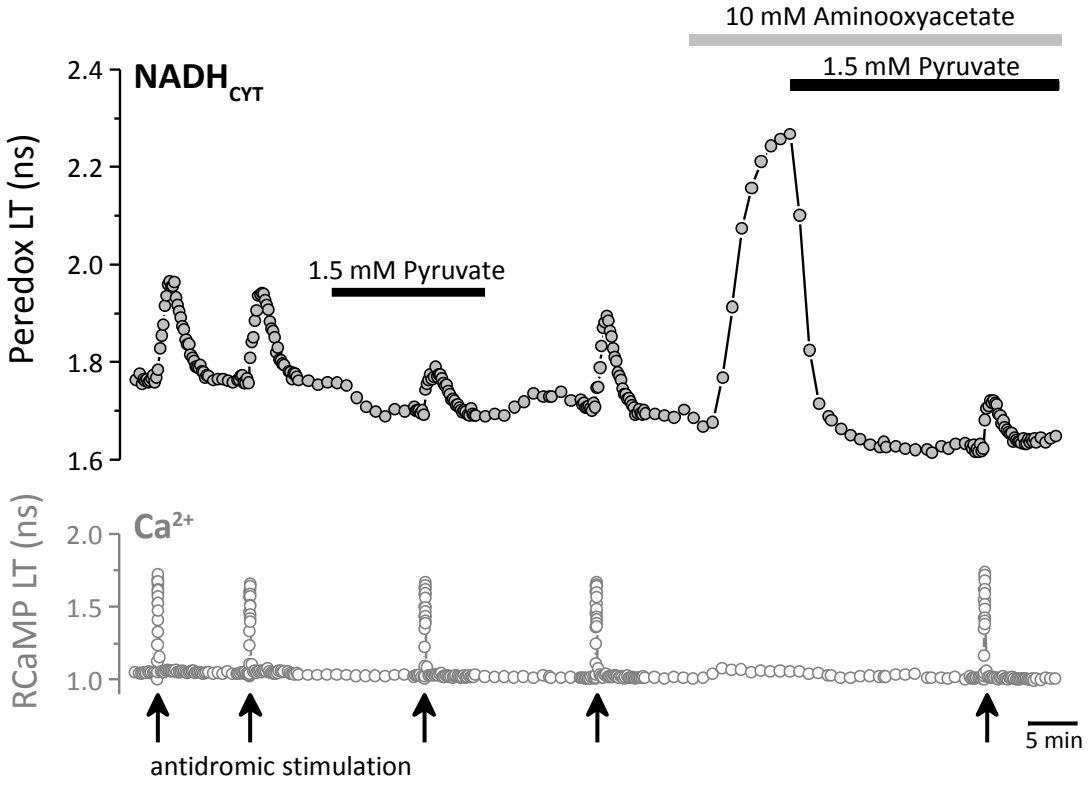

Figure S6. Inhibition of the mitochondrial malate-aspartate shuttle. Related to Fig. 6.

Representative trace of an experiment for MAS inhibition. After obtaining stable $NADH_{CYT}$ transients, a transient in the presence of 1.5 mM pyruvate was obtained as a control response for the test pulse after MAS inhibition. Washout of pyruvate was confirmed after the recovery of the baseline and also by another stimulation, which exhibited a response with a similar size to the initial transients. AOA was then applied until the effect of MAS blockade was evident as a rise in Peredox lifetime at baseline, which reached a value near saturation after 10 min. At this point, 1.5 mM pyruvate were added to the circulating ACSF+AOA and the baseline decreased and stabilized after 20 min. Antidromic stimulation produces $NADH_{CYT}$ transients in DGNs, still in the presence of AOA plus pyruvate.

The success of this experiment relied heavily on the timing of exposure to the different test conditions. To minimize delays because of perfusion exchange, the test compounds were added directly to the flask containing the ACSF recirculating in the chamber. Stock solutions were freshly prepared in ACSF the day of experiments, at 200X the concentration needed (i.e. 0.3 M for Na-Pyruvate). An aliquot equivalent to 0.5% of the recirculating volume was added to achieve the desired working concentrations. Picrotoxin (100 µM) was added to the ACSF (in addition to the iGluR blockers) to prevent potential effects due to AOA inhibition of GABA transaminase (McKenna et al., 2006).